

Classification of charge density waves based on their nature

Xuetao Zhu^{a,1}, Yanwei Cao^{a,1}, Jiandi Zhang^b, E. W. Plummer^{b,2}, and Jiandong Guo^{a,2}

^aBeijing National Laboratory for Condensed-Matter Physics and Institute of Physics, Chinese Academy of Sciences, Beijing 100190, China; and ^bDepartment of Physics and Astronomy, Louisiana State University, Baton Rouge, LA 70808

Contributed by E. W. Plummer, January 7, 2015 (sent for review August 15, 2014; reviewed by Takeshi Egami and Steven G. Louie)

The concept of a charge density wave (CDW) permeates much of condensed matter physics and chemistry. CDWs have their origin rooted in the instability of a one-dimensional system described by Peierls. The extension of this concept to reduced dimensional systems has led to the concept of Fermi surface nesting (FSN), which dictates the wave vector (\vec{q}_{CDW}) of the CDW and the corresponding lattice distortion. The idea is that segments of the Fermi contours are connected by \vec{q}_{CDW} , resulting in the effective screening of phonons inducing Kohn anomalies in their dispersion at \vec{q}_{CDW} , driving a lattice restructuring at low temperatures. There is growing theoretical and experimental evidence that this picture fails in many real systems and in fact it is the momentum dependence of the electron–phonon coupling (EPC) matrix element that determines the characteristic of the CDW phase. Based on the published results for the prototypical CDW system 2H-NbSe₂, we show how well the \vec{q} -dependent EPC matrix element, but not the FSN, can describe the origin of the CDW. We further demonstrate a procedure of combing electronic band and phonon measurements to extract the EPC matrix element, allowing the electronic states involved in the EPC to be identified. Thus, we show that a large EPC does not necessarily induce the CDW phase, with Bi₂Sr₂CaCu₂O_{8+δ} as the example, and the charge-ordered phenomena observed in various cuprates are not driven by FSN or EPC. To experimentally resolve the microscopic picture of EPC will lead to a fundamental change in the way we think about, write about, and classify charge density waves.

charge density wave | phonon | nesting

The phrase charge density wave (CDW) was first used by Fröhlich (1, 2) but originates from Peierls' description of a fundamental instability in a one-dimensional (1D) chain of atoms equally spaced by a lattice constant a (2). Fig. 1A shows the free electron band of such a 1D chain with one electron per atomic site. The Fermi points are at $k_F = \pm\pi/2a$ and are connected by the nesting vector $q = 2k_F$. In 1930 Peierls asserted that this system is unstable, showing an electronic disturbance with the wave vector $2k_F$, changing the periodicity of the chain, and opening up a gap at the zone boundary ($k = \pi/2a$) of the new unit cell containing two atoms (1, 2). The conjecture was that the gain in electronic energy would always overwhelm the cost of restructuring the atoms (1). Consequently in the Peierls model there would be a transition from the metallic high-temperature state to the insulating-dimerized ground state at a critical temperature T_{CDW} . Kohn (3) pointed out that there is an image of the Fermi surface in the vibrational spectrum, because the zero energy electronic excitations at $2k_F$ will effectively screen any lattice motion with this wave vector. Fig. 1B shows the phonon dispersion for this 1D chain at different temperatures (1). Below T_{CDW} the phonon energy at $q = 2k_F$ becomes imaginary, meaning there is a new lattice structure. Above T_{CDW} there is a sharp dip (Kohn anomaly) in the phonon dispersion but no static restructuring.

The question is how to extend the Peierls picture to real systems in higher dimensions (a real one-dimensional system is only quasi-1D). A standard practice is to calculate the susceptibility

$\chi(\vec{q}, \omega)$ for a given electronic configuration (1) and to use the zero energy value of the Lindhard response function $\chi_0(\vec{q}) \equiv \chi_0(\vec{q}, \omega = 0)$ (SI Text) to determine whether the electron response can drive a Peierls phase transition—there should be a peak in the imaginary part of the response function $\text{Im}[\chi_0(\vec{q})]$ at the Fermi surface nesting (FSN) vector \vec{q}_{CDW} as well as in the real part $\text{Re}[\chi_0(\vec{q})]$, because the real part defines the stability of the system (4). Fig. 1D shows the plot of $\text{Re}[\chi_0(\vec{q})]$ for a free electron system in 1D, 2D, and 3D (1), respectively, whereas Fig. 1C displays the free-electron Fermi contour in 2D. There is a logarithmic divergence in $\text{Re}[\chi_0(\vec{q})]$ for the 1D system but no peaks in the 2D and 3D electron gases. If CDWs are created by FSN, the Fermi contour must have been distorted to create nesting as represented by $\text{Re}[\chi_0(\vec{q})]$. In a seminal paper Johannes and Mazin demonstrated that the logarithmic divergence of $\text{Re}[\chi_0(\vec{q})]$ is not robust against small deviations from perfect nesting (4). The dotted line in Fig. 1D illustrates what happens for only a 2% deviation in k_F from perfect nesting and Fig. 1D, Inset, shows the effect of including a small “Drude relaxation” in the calculation for the susceptibility.

If FSN is the origin of the CDW as in the Peierls picture, the real and imaginary parts of the susceptibility calculated using the measured band structure should both show strong peaks at \vec{q}_{CDW} , there should be a Kohn anomaly in all of the phonons (except ones not allowed by symmetry) at \vec{q}_{CDW} (4), and at least one of the modes must go imaginary at low temperature, inducing a lattice distortion and an electronic gap. However, Johannes and Mazin argued, “only a tiny fraction if any, of the observed charge ordering phase transition are true analogs of the Peierls instability ...” (ref. 4, p. 1). In fact, it has been postulated that CDW phases are

Significance

Charge density waves (CDWs) are observed in many solids, especially in low-dimensional systems. Their existence was first predicted in the 1930s by Rudolf Peierls, who prophesied that CDWs would exist in an ideal one-dimensional (1D) chain of atoms, lowering the energy of the system and driving a reconstruction of the lattice. In 1959, Walter Kohn pointed out that this nesting results in what is now known as a “Kohn anomaly,” a simultaneous softening of coherent lattice vibrations, i.e., phonon softening. This simple textbook picture of the origin of CDWs does not seem to be correct in many materials and in this report we propose a previously unidentified classification of CDWs based upon their nature.

Author contributions: X.Z., Y.C., J.Z., E.W.P., and J.G. designed research; X.Z., Y.C., and J.G. performed research; X.Z., Y.C., J.Z., E.W.P., and J.G. analyzed data; and X.Z., J.Z., E.W.P., and J.G. wrote the paper.

Reviewers: T.E., University of Tennessee; and S.G.L., University of California, Berkeley.

The authors declare no conflict of interest.

Freely available online through the PNAS open access option.

¹X.Z. and Y.C. contributed equally to this work.

²To whom correspondence may be addressed. Email: wplummer@phys.lsu.edu or jdguo@iphys.ac.cn.

This article contains supporting information online at www.pnas.org/lookup/suppl/doi:10.1073/pnas.1424791112/-DCSupplemental.

illustrate that FSN is irrelevant and that the origin of the CDW state is tied to EPC (6, 7, 18–20). This realization should not have been a surprise because in 2004 Valla et al. reported that for NbSe₂ EPC was the dominant contribution to the renormalization of quasiparticle self-energy (22). Fig. 2A shows the Fermi contour obtained from a tight binding fit to the ARPES data (10, 12) and \vec{q}_{CDW} obtained from diffraction measurements (13, 14, 16, 17). Obviously there is no way to argue that the CDW arises from FSN! In fact, the absence of FSN can be seen in the real and imaginary parts of the susceptibility $\chi_0(\vec{q})$ plotted from the experimental data in the Γ –M direction in Fig. 2B and C. There is no sign of any structure at the FSN values of \vec{q}_{CDW} (FSN). Fig. 2D shows the STM image taken at 22 K (below T_{CDW}), with the Fourier transform shown in Fig. 2D, Inset (19). The arrow in Fig. 2D, Inset, marks the position of the periodicity of the electronic CDW that is the same as seen in the lattice distortion measured by diffraction (13, 14). Fig. 2E is the STM image at 96 K (above T_{CDW}), whose Fourier transform is missing the spot indicated in Fig. 2D, Inset. The structural transition order parameter is shown in Fig. 2F with the critical temperature at $T_{CDW} = 33.5$ K (17). Fig. 2G displays the measured resistivity as a function of temperatures, clearly showing the superconducting phase transition at T_S but almost no change at the CDW transition temperature T_{CDW} (21). There is no gap in the electronic system, i.e., no insulating state associated with the low-temperature CDW state, inconsistent with that predicted by the Peierls model.

Inelastic X-ray scattering reveals what appears to be a temperature-dependent Kohn anomaly in the acoustic phonon branch at \vec{q}_{CDW} (20). The data of the renormalized phonon dispersion along the Γ –M direction (Fig. 3A) (20) show the strong phonon softening located around $q_{CDW} \cong 0.695 \text{ \AA}^{-1}$, indicating the one-to-one correspondence between the CDW and the Kohn-like anomaly. Just below the transition temperature the phonon energy is imaginary, meaning there is a restructuring of the lattice. Above the transition temperature the phonon energy drops near \vec{q}_{CDW} but does not go to zero. Fig. 3B displays the phonon width as a function of q in the CDW phase at 33 K, showing an appreciable increase in width in the region of the phonon anomaly (20). This is a signature of the phonon coupling with other excitations in the system (EPC). Comparison of Fig. 3A with Fig. 1B shows that this is not a simple Kohn anomaly, because the phonon is damped over a considerable range of the BZ, in contrast to the sharp dip at $2k_F$ expected from FSN and the Peierls picture (20). The authors show by using ab initio calculations that the \vec{q} dependence of this phonon softening is dictated by EPC, not by FSN (20, 24), but they report little about the characteristics of the EPC coupling matrix element $|g(\vec{k}, \vec{k}')|^2$, presumably because they did not realize at the time that $|g(\vec{k}, \vec{k}')|^2$ could be measured experimentally. However, it can be determined experimentally as we will demonstrate, first for NbSe₂ and then for optimally doped cuprate Bi₂Sr₂CaCu₂O_{8+ δ} (Bi2212).

The \vec{q} -dependent EPC is described by the matrix element $|g(\vec{k}, \vec{k}')|^2$ that couples electronic states \vec{k} and \vec{k}' with a phonon of wave vector \vec{q} ($\vec{q} = \vec{k} - \vec{k}'$) and energy $\hbar\omega$ (25). If we make the assumption that $|g(\vec{k}, \vec{k}')|^2 = |g(\vec{q})|^2$, following Grimvall (25), we can determine $|g(\vec{q})|^2$ knowing $\text{Im}[\chi(q, \omega)]$ (8),

$$\Gamma_{\text{EPC}}(\vec{q}) = -2|g(\vec{q})|^2 \text{Im}[\chi(\omega, \vec{q})], \quad [1]$$

where $\Gamma_{\text{EPC}}(\vec{q})$ is the phonon linewidth. Ideally the interacting susceptibility $\text{Im}[\chi(q, \omega)]$, which carries the information from both electron–phonon and electron–electron interactions, should be used for the specific system being studied. However, experimentally it is not feasible to obtain the interacting $\text{Im}[\chi(q, \omega)]$. Thus, we have adapted an experimental approach, using the measured band structure, which contains both electron–phonon

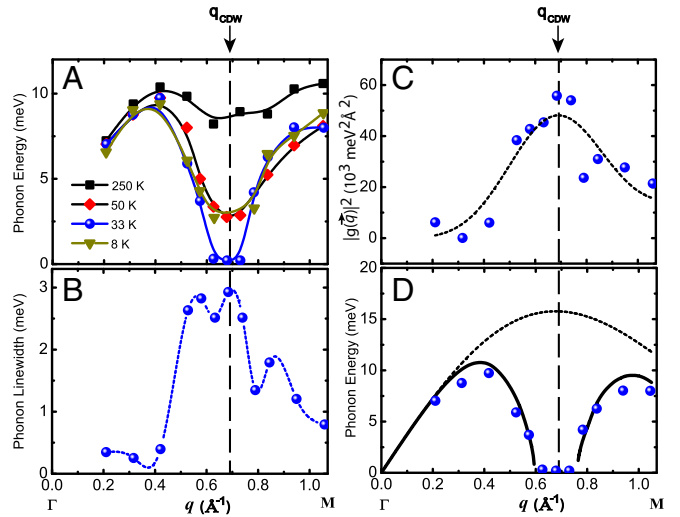


Fig. 3. Acoustic phonon softening in NbSe₂ along the Γ –M direction. (A) Measured phonon dispersion as a function of T (20). (B) Measured linewidth of the phonon at $T = 33$ K (20). (C) Extracted EPC matrix element $|g(\vec{q})|^2$ (text and Eq. 1). (D) Calculated soft phonon behavior (solid line), using $|g(\vec{q})|^2$ and an approximation for the bare phonon dispersion (dashed line).

and electron–electron coupling as the input to calculate the Lindhard response function $\text{Im}[\chi_0(q, \omega)]$. In the current case for an acoustic phonon, a good approximation is to use the zero energy value of the Lindhard function $\text{Im}[\chi_0(\omega, q)] = \text{Im}[\chi_0(0, q)] = \text{Im}[\chi_0(q)]$, which is plotted in Fig. 2C. The density-functional theory calculation in ref. (6) for the same system, including exchange–correlation interaction between electrons, obtained a very similar response function as shown from our procedure in figure 6 of ref. 6. This indicates that our experimental procedure is a reliable procedure for determining the response function. Fig. 3C shows the result of applying Eq. 1, using the best fit to $\Gamma_{\text{EPC}}(q)$ in the Γ –M direction (Fig. 3B and *SI Text*). It is clear, as anticipated, that the strong Kohn-like anomaly observed in 2H-NbSe₂ arises from the \vec{q} -dependent EPC matrix element with a peak at \vec{q}_{CDW} , not from the conventional FSN in the electronic structure. A consistency check can be performed by using the extracted $|g(\vec{q})|^2$ in the equation derived by Grimvall (25), relating the measured phonon dispersion $\omega(\vec{q})$ to the bare phonon dispersion $\omega_0(\vec{q})$ (without EPC):

$$\omega(\vec{q})^2 = \omega_0(\vec{q})^2 + 2\omega_0(\vec{q})|g(\vec{q})|^2 \text{Re}[\chi(\omega, \vec{q})]. \quad [2]$$

Replacing $\text{Re}[\chi(\omega, \vec{q})]$ with the zero-frequency limit $\text{Re}[\chi_0(\vec{q})]$ plotted in Fig. 2B gives the result displayed in Fig. 3D, where we have approximated $\omega_0(\vec{q})$ by extrapolating the high-temperature data shown in Fig. 3A. The predicted acoustic phonon dispersion (solid lines) is in remarkable agreement with the data (20). This example illustrates how important the measurements of phonon dispersion and linewidth are in unraveling the origin of the CDWs in the metallic crystals. However, there are still questions remaining. For example, will a large $|g(\vec{q})|^2$ always lead to the formation of a CDW state with lattice distortion? If not, why?

To answer this question we examine systems with large EPC but very different electronic behavior, such as cuprates. The fact that cuprates belong to the class of unconventional superconductors is not immediately relevant to this study. However, in cuprates, different charge-ordering (CO) phenomena have been reported, such as a stripe phase in La_{1.6-x}Nd_{0.4}Sr_xCuO₄ (26, 27), a checkerboard phase (28, 29) and a special kind of short-range CO phase (30, 31) in Bi2212, and long-range charge fluctuations (32) or CDWs (33, 34) in YBa₂Cu₃O_{6+x} (YBCO). The competition

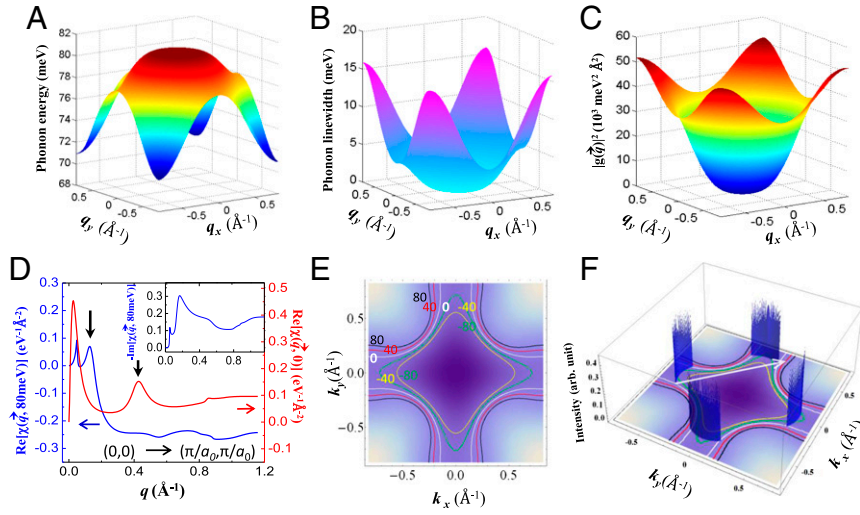


Fig. 4. EPC associated with apical oxygen A_{1g} phonon mode in optimally doped $\text{Bi}_2\text{Sr}_2\text{CaCu}_2\text{O}_{8+\delta}$. (A) Fit to the measured phonon dispersion (8). (B) Fit to the measured linewidth as a function of momentum (8). (C) $|g(\vec{q})|^2$ extracted from the phonon and ARPES data (8, 40). (D) Calculated $\text{Re}\chi(\vec{q}, \omega)$ for $\omega = 0$ meV and 80 meV from the ARPES data along the $(0,0) \rightarrow (\pi/a_0, \pi/a_0)$ direction. *Inset* shows the calculated $\text{Im}\chi(\vec{q}, \omega)$ for 80 meV. (E) Constant energy contours within 80 meV of the Fermi surface (40). (F) Density of possible initial states \vec{k} calculated with $|g(\vec{q})|^2$ in C, where the final states \vec{k}' are above the Fermi level and the initial and final electronic states are separated by $\vec{q} = (\pi/a_0, \pi/a_0) = (0.822 \text{ \AA}^{-1}, 0.822 \text{ \AA}^{-1})$ (white arrow) with the phonon energy $\hbar\omega$.

between these CO phases and magnetic ordering and superconductivity (35) continues to attract intensive interest within the community. Comin et al. pointed out that the simple FSN near the antinodal region is not the driving force of the CO (36). Recent phonon measurements (37, 38) show signatures of strong EPC in the low-temperature (below 150 K) charge-ordering phase of YBCO. However, the role of EPC in YBCO is substantially different from the role in NbSe_2 due to two aspects: (i) No phonon softening was observed above 150 K (T_{CDW}) and (ii) the energy of the soft phonon modes never approaches zero. Thus, EPC is not strong enough in cuprates to drive the formation of the CO or CDW phase. Unlike the case in 2D layered materials like NbSe_2 , neither FSN nor EPC is directly relevant to the CO or CDW phases in cuprates. A recent STM study (39) clearly demonstrated that the observed modulations of the electronic structure in cuprates are unconventional density waves, where antiferromagnetic and Coulomb interactions may play a key role. In any case whatever the CO phase in cuprates is, it is not a conventional CDW.

We use optimally doped Bi2212, a typical quasi-2D cuprate with large EPC, as an example, to illustrate the different role of EPC in cuprates. Here a whole set of data exists, specifically for the apical oxygen A_{1g} out-of-plane optical phonon mode (8). Fig. 4A plots our fit to the measured dispersion of the optical phonon branch at ~ 80 meV (8), showing a rapid downward dispersion for momentum larger than $\sim 0.41 \text{ \AA}^{-1}$, especially in the $(0,0) \rightarrow (\pi/a_0, \pi/a_0)$ direction ($a_0 = 3.82 \text{ \AA}$ denotes the in-plane lattice constant of Bi2212). Our fit to the linewidth data (9), shown in Fig. 4B, reveals that this downward dispersion is a result of many-body coupling in this system; i.e., the linewidth increases dramatically in the regions of large downward dispersion. Fig. 4C shows the EPC matrix element $|g(\vec{q})|^2$ of this mode calculated by using published ARPES data that determine $\chi(\vec{q}, \omega)$ (40) and the fit to the reported phonon dispersion and linewidth (8). Different from the case of NbSe_2 , the peak in $|g(\vec{q})|^2$ of Bi2212 is at the zone boundary $(\pi/a_0, \pi/a_0)$, which if large enough in magnitude would have driven the phonon energy imaginary, resulting in a commensurate reconstruction, i.e., a $(\sqrt{2} \times \sqrt{2})R45^\circ$ superstructure that has been reported for Sr_2RuO_4 when a phonon goes soft at the zone boundary (41). Note that the maximum in $|g(\vec{q})|^2$ is $\sim 50 \times 10^3 \text{ meV}^2 \cdot \text{\AA}^{-2}$ for both NbSe_2 (Fig. 3C) and Bi2212 (Fig. 4C).

Knowing $|g(\vec{q})|^2$, can we answer the question, Why is there a CDW associated with a Kohn-like anomaly in NbSe_2 but not with the A_{1g} optical phonon mode in Bi2212? When the phonon mode is imaginary at \vec{q}_{CDW} [$\omega^2(\vec{q}_{\text{CDW}}) \leq 0$], Eq. 2 gives

$$|g(\vec{q}_{\text{CDW}})|^2 \cong \frac{\omega_0(\vec{q}_{\text{CDW}})}{2|\text{Re}[\chi(\vec{q}_{\text{CDW}}, \omega)]}. \quad [3]$$

For NbSe_2 the critical value of $|g(\vec{q})|^2$ is approximately given by $|g_{\text{crit}}(\vec{q}_{\text{CDW}})|^2 \approx 15 \text{ meV}/2(0.16 \text{ eV}^{-1} \cdot \text{\AA}^{-2}) = 48 \times 10^3 \text{ meV}^2 \cdot \text{\AA}^{-2}$, but for Bi2212 it is $|g_{\text{crit}}(\vec{q}_{\text{CDW}})|^2 \approx 80 \text{ meV}/2(0.25 \text{ eV}^{-1} \cdot \text{\AA}^{-2}) = 160 \times 10^3 \text{ meV}^2 \cdot \text{\AA}^{-2}$. Obviously the oxygen A_{1g} phonon mode in Bi2212 does not go to zero because the energy is too large. If there is an incipient CDW instability in a cuprate that is associated with EPC, then there must be a low-energy phonon whose energy becomes imaginary (32).

Why is the shape of the EPC matrix element in Bi2212 so different from that in NbSe_2 ? A full understanding will come only when we understand the microscopic picture of the coupling between specific phonons and electronic states of the system; i.e., Which states contribute to $|g(\vec{q})|^2$ at any \vec{q} ? To evaluate the contributions from the electronic bands to $|g(\vec{q})|^2$ in Bi2212, we plot in Fig. 4D both $\text{Re}[\chi(\vec{q}, 0)]$ and $\text{Re}[\chi(\vec{q}, 80 \text{ meV})]$ in the $(0,0) \rightarrow (\pi/a_0, \pi/a_0)$ direction, illustrating their dramatic difference with energy. One might have argued from $\text{Re}[\chi(\vec{q}, 0)]$ that this system would support a CDW at $q \sim 0.41 \text{ \AA}^{-1}$ because of the peak at this momentum, but there is no peak in $\text{Re}[\chi(\vec{q}, 80 \text{ meV})]$ at this momentum. Fig. 4D, *Inset*, shows $\text{Im}[\chi(\vec{q}, 80 \text{ meV})]$ with a peak at $q \sim 0.18 \text{ \AA}^{-1}$, which is also present in $\text{Re}[\chi(\vec{q}, 80 \text{ meV})]$, indicating that there could be a Kohn-like anomaly in the A_{1g} phonon branch at this q . However, in fact nothing is seen in the phonon dispersion or linewidth at this small q (Fig. 4A and B). Here again it is illustrated that although the shape of the susceptibility function is important for determining the characteristics of $|g(\vec{k}, \vec{k}')|^2$, it appears to have little predictive power when it comes to predicting the existence of or the characteristic of a CDW (4).

To gain insight into the microscopic picture of EPC for this specific phonon, we must learn which states contribute to $|g(\vec{q})|^2$

at a given \vec{q} . In Fig. 4E we show the contour plot of the electronic band within the phonon energy range near Fermi energy (0 ± 80 meV) (40). Note how slowly the band disperses in the $(0, 0) \rightarrow (\pi/a_0, 0)$ direction near the BZ boundary, in contrast to that in the $(0, 0) \rightarrow (\pi/a_0, \pi/a_0)$ direction. The initial electron states contributing to the susceptibility functions are mainly located in this region of k space. This is why the susceptibility functions shown in Fig. 4D are so dependent upon ω and obviously influence the shape of $|g(\vec{q})|^2$. To illustrate this, we select the momentum $\vec{q} = (\pi/a_0, \pi/a_0) = (0.822 \text{ \AA}^{-1}, 0.822 \text{ \AA}^{-1})$, where $|g(\vec{q})|^2$ has its maximum value (Fig. 4C), and plot the relative density of initial states contributing to $|g(\vec{q})|^2$ (SI Text) in Fig. 4F. Allowed initial states along the vector $\vec{k} = (k_x, 0)$ are only within a very narrow range of momentum and energy (conservation of energy and momentum), from $k_x = 0.632 \text{ \AA}^{-1}$ to 0.638 \AA^{-1} and 74.4 meV to 79.7 meV, respectively. Because of the flat band characteristic in the $(0, 0) \rightarrow (\pi/a_0, 0)$ direction (Fig. 4E), these allowed initial states are indeed far from the Fermi contour. In SI Text we show the plot for $\vec{q} = (\pi/a_0, 0) = (0.822 \text{ \AA}^{-1}, 0)$, which is dramatically different from that in Fig. 4F.

In summary, we have illustrated in this paper how to experimentally determine the details contained in the EPC matrix element by combining measurements of the electron band dispersion with those of the phonon dispersion and linewidth. The contribution of specific electronic and vibrational states can be identified. For those materials where EPC dictates the CDW wave vector, this procedure should lead to a new understanding of the origin and the effect of CDWs in solids. There are two important additional questions yet to be answered (especially from the aspect of theoretical modeling): What determines the characteristics of the EPC matrix element and why? It is worth

pointing out that the proposed procedure will not work for all systems, because of the basic physics associated with different classes of CDW. The concept of a CDW has been applied to many materials without a clear definition of the essence of the CDW. We suggest that there are at least three types of CDWs. Type I CDWs are quasi-1D systems with their origin in the Peierls instability (FSN). Here the lattice distortion is a secondary effect (4) and results from the electronic disturbance. The best example may be linear chain compounds (1). Type II CDWs are driven by EPC but not by FSN. Here the electronic and lattice instabilities are intimately tied to each other, and there is a phonon mode at \vec{q}_{CDW} going to zero at the transition temperature T_{CDW} . There is no reason to have a metal-insulator transition associated with the transition. Type II CDWs have been described in this paper with NbSe₂ as the example. Type III CDWs are systems where there is a charge modulation (or CO) with no indication of FSN or EPC as the driving force. The best example of type III CDWs may be the cuprates that exhibit CO phenomena (26–39). Strong EPC or FSN may exist in those systems, but there is no clear signature that EPC or FSN is essential to the formation of the CDWs. We emphasize that measurement of phonon dispersion and linewidth coupled with electron spectroscopy is the way to classify the types of CDWs and to understand their origin. This is especially true for type III systems where the origin of or even the existence of CDWs is still under debate (42).

ACKNOWLEDGMENTS. We thank Drs. John Tranquada and Igor Mazin for their comments on the manuscript. We also thank Drs. C. J. Arguello, S. P. Chockalingam, and A. N. Pasupathy for sharing their scanning tunneling microscopy images of NbSe₂. This research was funded by the 973 Project (2012CB921700), the Natural Science Foundation of China (11225422 and 11304367), and the External Cooperation Program of the Bureau of International Cooperation, Chinese Academy of Sciences (112111KYSB20130007).

- Gruner G (1994) *Density Waves in Solids* (Addison-Wesley, Reading, MA).
- Peierls RE (1955) *Quantum Theory of Solids* (Oxford Univ Press, New York).
- Kohn W (1959) Image of the Fermi surface in the vibration spectrum of a metal. *Phys Rev Lett* 2(9):393–394.
- Johannes MD, Mazin II (2008) Fermi surface nesting and the origin of charge density waves in metals. *Phys Rev B* 77(16):165135.
- Varma C, Simons A (1983) Strong-coupling theory of charge-density-wave transitions. *Phys Rev Lett* 51(2):138.
- Johannes MD, Mazin II, Howells CA (2006) Fermi-surface nesting and the origin of the charge-density wave in NbSe₂. *Phys Rev B* 73(20):205102.
- Calandra M, Mazin II, Mauri F (2009) Effect of dimensionality on the charge-density wave in few-layer 2H-NbSe₂. *Phys Rev B* 80(24):241108.
- Qin H, et al. (2010) Direct determination of the electron-phonon coupling matrix element in a correlated system. *Phys Rev Lett* 105(25):256402.
- Peierls RE (1991) *More Surprises in Theoretical Physics* (Princeton Univ Press, Princeton), p 29.
- Inosov DS, et al. (2008) Fermi surface nesting in several transition metal dichalcogenides. *New J Phys* 10:12507.
- Borisenko SV, et al. (2008) Pseudogap and charge density waves in two dimensions. *Phys Rev Lett* 100(19):196402.
- Borisenko SV, et al. (2009) Two energy gaps and Fermi-surface “arcs” in NbSe₂. *Phys Rev Lett* 102(16):166402.
- Singh O, Curzon A (1976) An electron diffraction evidence of charge density wave instability in 2H-NbSe₂. *Phys Lett A* 56(1):63–64.
- Chen C (1984) Electron diffraction study of the charge-density wave superlattice in 2H-NbSe₂. *Solid State Commun* 49(7):645–647.
- Du CH, et al. (2000) X-ray scattering studies of 2H-NbSe₂, a superconductor and charge density wave material, under high external magnetic fields. *J Phys Condens Matter* 12(25):5361–5370.
- Moncton DE, Axe JD, Disalvo FJ (1975) Study of superlattice formation in 2H-NbSe₂ and 2H-TaSe₂ by neutron-scattering. *Phys Rev Lett* 34(12):734–737.
- Moncton DE, Axe JD, Disalvo FJ (1977) Neutron-scattering study of charge-density wave transitions in 2H-TaSe₂ and 2H-NbSe₂. *Phys Rev B* 16(2):801–819.
- Soumyanarayanan A, et al. (2013) Quantum phase transition from triangular to stripe charge order in NbSe₂. *Proc Natl Acad Sci USA* 110(5):1623–1627.
- Arguello CJ, et al. (2014) Visualizing the charge density wave transition in 2H-NbSe₂ in real space. *Phys Rev B* 89(23):235115.
- Weber F, et al. (2011) Extended phonon collapse and the origin of the charge-density wave in 2H-NbSe₂. *Phys Rev Lett* 107(10):107403.
- Naito M, Tanaka S (1982) Electrical transport properties in 2H-NbSe₂, 2H-NbSe₂, 2H-TaSe₂ and 2H-TaSe₂. *J Phys Soc Jpn* 51(1):219–227.
- Valla T, et al. (2004) Quasiparticle spectra, charge-density waves, superconductivity, and electron-phonon coupling in 2H-NbSe₂. *Phys Rev Lett* 92(8):086401.
- Gruner G (1988) The dynamics of charge-density waves. *Rev Mod Phys* 60(4):1129–1182.
- Weber F, et al. (2013) Optical phonons and the soft mode in 2H-NbSe₂. *Phys Rev B* 87(24):245111.
- Grimvall G (1981) *The Electron-Phonon Interaction in Metals* (North-Holland, Amsterdam).
- Tranquada J, Sternlieb B, Axe J, Nakamura Y, Uchida S (1995) Evidence for stripe correlations of spins and holes in copper oxide superconductors. *Nature* 375(6532):561–563.
- Kivelson SA, et al. (2003) How to detect fluctuating stripes in the high-temperature superconductors. *Rev Mod Phys* 75(4):1201–1241.
- Hoffman JE, et al. (2002) A four unit cell periodic pattern of quasi-particle states surrounding vortex cores in Bi₂Sr₂CaCu₂O_{8+δ}. *Science* 295(5554):466–469.
- Wise W, et al. (2008) Charge-density-wave origin of cuprate checkerboard visualized by scanning tunnelling microscopy. *Nat Phys* 4(9):696–699.
- da Silva Neto EH, et al. (2014) Ubiquitous interplay between charge ordering and high-temperature superconductivity in cuprates. *Science* 343(6169):393–396.
- Hashimoto M, et al. (2014) Direct observation of bulk charge modulations in optimally doped Bi_{1.5}Pb_{0.5}Sr_{1.5}CaCu₂O_{8+δ}. *Phys Rev B* 89(22):220511(R).
- Ghiringhelli G, et al. (2012) Long-range incommensurate charge fluctuations in (Y,Nd)Ba₂Cu₃O_(6+x). *Science* 337(6096):821–825.
- Chang J, et al. (2012) Direct observation of competition between superconductivity and charge density wave order in YBa₂Cu₃O_{6.67}. *Nat Phys* 8(12):871–876.
- Blackburn E, et al. (2013) X-ray diffraction observations of a charge-density-wave order in superconducting ortho-II YBa₂Cu₃O_{6.54} single crystals in zero magnetic field. *Phys Rev Lett* 110(13):137004.
- Gabovich A, et al. (2010) Competition of superconductivity and charge density waves in cuprates: Recent evidence and interpretation. *Adv Condens Matter Phys* 2010:681070.
- Comin R, et al. (2014) Charge order driven by Fermi-arc instability in Bi₂Sr_{2-x}La_xCuO_{6+δ}. *Science* 343(6169):390–392.
- Blackburn E, et al. (2013) Inelastic x-ray study of phonon broadening and charge-density wave formation in ortho-II-ordered YBa₂Cu₃O_{6.54}. *Phys Rev B* 88(5):054506.
- Le Tacon M, et al. (2014) Inelastic X-ray scattering in YBa₂Cu₃O_{6.6} reveals giant phonon anomalies and elastic central peak due to charge-density-wave formation. *Nat Phys* 10(1):52–58.
- Fujita K, et al. (2014) Direct phase-sensitive identification of a d-form factor density wave in underdoped cuprates. *Proc Natl Acad Sci USA* 111(30):E3026–E3032.
- Norman MR, Randeria M, Ding H, Campuzano JC (1995) Phenomenological models for the gap anisotropy of Bi₂Sr₂CaCu₂O₈ as measured by angle-resolved photoemission spectroscopy. *Phys Rev B Condens Matter* 52(1):615–622.
- Matzdorf R, et al. (2000) Ferromagnetism stabilized by lattice distortion at the surface of the p-wave superconductor Sr(2)RuO₄. *Science* 289(5480):746–748.
- Plakida N (2010) *High-Temperature Cuprate Superconductors: Experiment, Theory, and Applications* (Springer, Berlin), pp 349–376.